KU LEUVEN

Instabilities in Cortical Networks with Embedded Synfire Chains

Maxime Lucas

Thesis submitted for the degree of Master of Science in Artificial Intelligence, option Engineering and Computer Science

Thesis supervisor:
Prof. Dr. Cees van Leeuwen

Academic year 2014 – 2015

KU LEUVEN

Instabilities in Cortical Networks with Embedded Synfire Chains

Maxime Lucas

Thesis submitted for the degree of Master of Science in Artificial Intelligence, option Engineering and Computer Science

Thesis supervisor:
Prof. Dr. Cees van Leeuwen

Assessors:
Dr. Tomer Fekete
Dr. Chris Trengove

Mentor:
Dr. Chris Trengove, Daily supervisor

Academic year 2014 – 2015

Master thesis filing card

Student: Maxime Lucas

Title: Instabilities in Cortical Networks with Embedded Synfire Chains

Dutch title: Instabiliteiten in Corticale Netwerken met daarin Verankerde Synfire Chains

UDC: 681.3*I20

Abstract:

Precisely timed firing patterns of cortical neurons are explained by sequences of feed-forward connections of pools of neurons – synfire chains. Several embedding strategies into cortex-like networks for those structures have been proposed, and their properties have been investigated. We go a step further than [25]: we use model neurons with a non-instantaneous integration of synaptic input current. Given this incremental modification, we explore the state space of the new model, seeking instabilities. We study the equilibrium states of the system using numerical simulations. We show that the equilibrium firing rates observed are well described by a mean field analysis, for a large range of the parameters considered. We also show that, when synaptic inhibition strength and the size of the pools of neurons are sufficiently low, the system reaches a state dominated by spikes due to random fluctuations of their membrane potential, rather than by propagation of volleys of spikes – synfire waves – along the synfire chains. We explain this novel regime in terms of the mean field analysis, by means of the non-monotonic transfer function of our neurons. Moreover, we show the appearance of spontaneous wave births at high pool sizes. Finally, we show that non-instantaneous synapses are sufficient for a regulation of the number of co-active waves to occur, so that variable pool-to-pool transmission delays are no longer required.

Thesis submitted for the degree of Master of Science in Artificial Intelligence, option Engineering and Computer Science

Thesis supervisor: Prof. Dr. Cees van Leeuwen

Assessors: Dr. Tomer Fekete
Dr. Chris Trengove

Mentor: Dr. Chris Trengove, Daily supervisor

1 Introduction

How information is encoded in our brain has been a rich question for decades now. Among different models for information encoding in the brain, one of the simplest and most commonly accepted is that information is encoded in the firing rate of a population of neurons. In 1982, however, Abeles showed the existence of precisely timed firing patterns, suggesting the need for a more complex underlying model for information encoding [4] (and later, e.g [1]). Multiple neurons were recorded simultaneously *in vivo*, and correlations of the spiking times between pairs and triplets of neurons were examined. Correlation between pairs could be explained on the basis of simple known connexions between pairs of neurones, but some patterns found in triplets could not. It appeared that precise firing patterns occurred more often than chance level would allow. The precise repetition of those patterns, and the time periods – tens to hundreds of milliseconds – over which they take place lead Abeles to suggest a new network structure to account for them: synfire chains (SFCs).

An SFC's structure is as follows: a chain of pools of neurons, linked up by excitatory feed-forward links. Some or all neurons in a pool are connected to those in the next. The properties of single neurons allow this structure to propagate quasi-simultaneous volleys of spikes from one pool to the next ; indeed, the more excitatory inputs a neuron receives simultaneously, the more likely it is to produce a spike in response. Hence, if sufficiently many neurons in a pool happen to fire in a small time interval, the neurons in the next pool are highly likely to spike in response, and the pulse packet will propagate through the chain.

Such structures are interesting for several reasons, one of them being that compositional cognitive representation systems can be achieved by linking several SFCs together and it could well be that the brain acts as such a compositional system (e.g. [22]). Compositionality is the simple idea of building complex objects or representations from their parts. Evidence of such primitive parts has been found in complex movement tasks, with the directionality specificity of neurons in grasping-monkey experiments (see [12]) regarded as its simplest illustration. How such compositional activities could be realised in the brain is still an open question [22], to which SFCs could help providing an answer. In such systems, SFCs are dynamically linked together, and the activation patterns of the chains depends on the stimuli.

Certain dynamical properties of SFCs have been identified as critical for their functional relevance. First, stable propagation of waves – both in size of pulse packets and in time spread – was shown to be possible only above a critical pool size [11, 15]. A second critical property is the so-called stability of the ground state. This ground state of SFC models is that where its neurons exhibit cortex-like AI (asynchronous irregular) activity, as referred to by Brunel [7]. The ground state stands in contrast to the excited state, in

which volleys of synchronous spikes propagate. Normally, the excited state is induced, and there is no spontaneous wave births ; ground state instability is the situation in which volleys of propagating waves appear spontaneously. It was first shown that this ground state can become unstable above an upper bound on pool size in [23].

Once SFCs alone had been studied, the next step was to embed them in a cortex-like network in order to be more realistic. This goal was first pursued in [6], where a SFC was embedded in a balanced random network (BRN). A BRN, best exemplified by [7], is a type of network where connections are randomly and sparsely drawn between two populations of neurons – one excitatory, and one inhibitory. Such an architecture was shown to exhibit a low rate AI regime – of the order of 1-5 Hz, when driven by external excitation, provided recurrent inhibition is sufficiently strong. In that kind of network, the spiking of neurons may be referred to as stochastic since spikes occur from random or quasi-random fluctuations in the membrane potentials of neurons. Various SFC embedding strategies [20, 22] have been used with different aims, e.g. to include anatomically-based spatial constraints [20], or to strengthen the robustness of wave propagation with so-called shadow pools [5]. The latter strategy was also used in [25]. An SFC embedding model may replace just some of the excitatory connections in the BRN with synfire chain connections [6, 17, 20] or all of them [22, 25]. In the latter, the random sparse connectivity arises from the random selection of pools.

The present study is based on the SFC embedding model of [25], which exhibits a number of favourable properties. The model exhibits stable propagation of waves and a stable ground state for the same parameters, but mainly focuses on the embedding capacity possibly achievable by such a system, and sets a new record for it. The embedding capacity involves not only the number of embedded pools, but also the number of waves that can co-exist in the system, a trade-off existing between the two. A high embedding capacity is a desirable property for functionally relevant SFC systems, as combinatorial representations can be powerful only if the number of primitives activated in the system can be significant. Self-regulation of the number of co-active waves in the system is another desirable stability property that the model in [25] exhibits. These advantageous properties are attributed to three distinctive features of the model. First, conductance-based synapses rather than current-based ones, allowing a better trade-off between stabilising wave propagation and minimising stochastic spiking. Second, so-called inhibitory "shadow" pools of neurons, linked to chains so as to keep the balance of excitation and inhibition in total activity and recurrent background input. Finally, variability in the transmission delays of connections linking one pool to the next, so as to facilitate self-regulation of wave activity.

In this study, we further the work of [25] in several ways. First, we replace the instantaneous synapses by non-instantaneous ones. Such a modification was suggested in [25] to have the same effect on the regulation of the number of waves as that of variabilty in intra-link transmission delays, such as was present in [25]. Second, we go further in the

exploration of the plane of parameters generated by pool-size and inhibitory synaptic strength. More importantly, the focus is different: we look for possible instabilities in the system as we push the values of the parameters. Indeed, it has been shown [7, 19] that reducing inhibition may put the balanced recurrent network outside the inhibition-dominated regime in which the AI state of low-rate stochastic spiking persists. It was found in [25] that there was an optimum inhibition level which optimised a trade-off between promoting synfire wave propagation and limiting stochastic spiking. As to pool size, it has an effect on the stability of wave propagation and that of the ground state of the SFC, as mentioned earlier. Tuning those two parameters, several instabilities are possible: loss of regulation of the number of waves, transition into a high rate state of stochastic spiking, with no means for waves to propagate, or loss of ground state stability – *i.e.* spontaneous births of waves. We conduct the study using both numerical simulations and a theoretical mean field analysis. We show that such a mean field description gives good predictions for the equilibrium values of the macroscopic quantities of the system. The aim of the study as a whole is a better understanding of the phase diagram of the system and how it changes due to the use of non-instantaneous synapses.

The present document is divided in three parts. In section 2 , we present the details of the model, and introduce the numerical techniques used for its simulations and analysis. The mean field approach is also described. We present the results of the network simulations and the mean field analysis in section 3. Finally, in section 4 , we discuss those results before making concluding remarks and planning for future work.

2 Methods and models

2.1 Synfire chain superposition network (SFCSN)

2.1.1 Network model

The network model studied is based on that proposed in [25] and is illustrated in figure 1(a). It consists of two populations of neurons, one composed of N_E excitatory neurons, the other is composed of N_I inhibitory neurons. Neurons are then drawn randomly from those populations to form p pools. An excitatory pool is composed of n_E distinct neurons, and likewise an inhibitory one is composed of n_I distinct ones. Note that one neuron can belong to more than one pool. Indeed, since the total number of allocations of neurons to pools is pn_E, one neuron belongs on average to pn_E/N_E. To ensure that every neuron appears in about the same number pools, it is required that each neuron appears in either $\lfloor pn_E/N_E \rfloor$ or $\lceil pn_E/N_E \rceil$ pools, which yields the wished average. Note that although we refer to p as the number of pools, there are actually p excitatory and p inhibitory pools, yielding $2p$ pools. However, only excitatory pools are necessary for synfire wave propagation, and we usually thus only refer to those p pools.

After creation of the pools, chains need to be built from them. This can be done in numerous ways, by choosing to either build fewer long chains or more small chains, keeping in mind that a pool can only belong to a single chain. In our model, as in [25], the model has a single circular chain composed of all p pools, i.e. pool p is linked to pool 1. Consecutive excitatory pools in the chain are linked by linking all the neurons of the first pool to all those in the next, in an all-to-all fashion. Each excitatory pool is also linked to the next inhibitory pool. Note that these are the only excitatory connections present in the network. The fact that one neuron belongs to several pools makes the network recurrent. In fact, ignoring their pool-specific correlations, the excitatory connections resemble those of a balanced random network. This is the basis of our mean field analysis (see section 2.2).

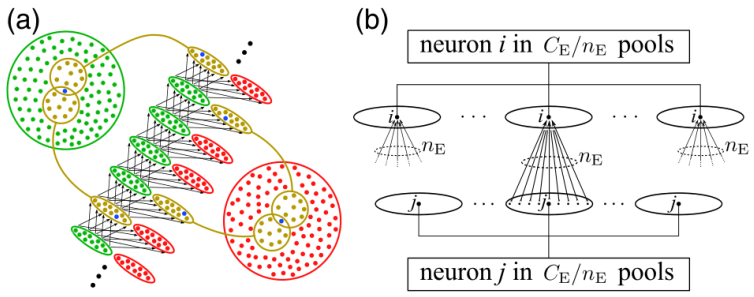

Figure 1: Chain embedding model. Image from [25].

A particular excitatory neuron receives input from all n_E neurons from the preceding excitatory pool, and that is true for all $\lfloor pn_E/N_E \rfloor$ or $\lceil pn_E/N_E \rceil$ pools it appears in. Hence, it receives input from either $\lfloor pn_E/N_E \rfloor n_E$ or $\lceil pn_E/N_E \rceil n_E$, which is an average connectivity of

$$C_E = pn_E^2/N_E. \tag{1}$$

The more biologically meaningful quantities of our system are C_E and the sparseness ϵ, *i.e.* the fraction of the total number of neurons that a neuron receives on average as input: $C_E = \epsilon N_E$. Hence, in the simulations we set C_E and ϵ along with n_E, and derive other relevant parameters such as N_E and p from them.

Similar reasoning leads to the average number of connections an inhibitory neuron receives being $(pn_I/N_I)n_E$. We further assume in the model that the following I/E ratios are all equal to the same constant value: $n_I/N_E = N_I/N_E = \gamma$. This ensures, among other things, that the inhibitory and excitatory neurons receive the same mean number of excitatory pre-synaptic connections, both being C_E. As for input from inhibitory neurons, the number of inhibitory connections every neuron receives is set to a fixed fraction of its number of excitatory pre-synaptic connections. These connections are drawn randomly from the population of inhibitory neurons. For simplicity, we set the fraction to γ, and hence the mean number of pre-synaptic inhibitory neurons per neuron is $C_I = \gamma C_E$.

2.1.2 Neuron and synapse model

We use leaky integrate-and-fire (IAF) neurons with conductance-based synapses. This is similar to [25], but there is one important difference: in [25], the synaptic conductance response to an incoming spike is instantaneous (*i.e.* impulsive) whereas in the present model, the response is non-instantaneous. This means that a spike induces a transient conductance response which decays over time, which is is more realistic. We choose an exponential function to render that non-instantaneous character. Leaky (IAF) neurons are described by the sub-threshold dynamics of their membrane potential $V(t)$

$$\frac{\mathrm{d}V}{\mathrm{d}t} = \frac{1}{\tau_m}[V_{rest} - V(t)] + \frac{1}{C} I_{syn}(t), \tag{2}$$

in terms of the membrane time constant τ_m, the resting potential V_{rest} of the neuron, the membrane capacitance C, and the electric current $I_{syn}(t)$ due to synaptic inputs. Whenever the membrane potential goes higher than the threshold potential V_θ, it is set to the reset potential V_R and the neuron emits a spike. After that, the neuron is prevented from firing for a period of time called refractory and denoted t_{ref}.

The total synaptic current received by a neuron from both excitatory and inhibitory synapses can be written as

$$I_{syn}(t) = I_{syn}^I(t) + I_{syn}^E(t). \tag{3}$$

Conductance-based synapses, as opposed to current-based ones, have a voltage-dependent current response of the form $(V_x - V(t))g^x_{syn}(t)$ where x stands for either I or E , and V_x and $g^x_{syn}(t)$ are respectively the reversal potential and the conductance response associated to the type of synapse. Different such $g^x_{syn}(t)$ functions can be chosen among those describing either instantaneous synapses or non-instantaneous ones. In this study, we choose a function of the form $g^x_{syn}(t) = \exp(-t/\tau^x_{syn})$. The total current of type x is the sum of all the current responses to incoming events at type x synapses, and can thus be written

$$I^x_{syn}(t) = [V_x - V(t)] \sum_{i,j} \Theta(t - t_{i,j}) G_x \exp[-(t - t_{i,j})/\tau^x_{syn}], \tag{4}$$

where $t_{i,j}$ denotes the jth spiking time of the ith pre-synaptic neuron, and $\Theta(t)$ refers to the Heaviside function, which is 1 for positive values of t and 0 otherwise. The shape of the synaptic conductance response $g^x_{syn}(t)$ is thus determined in time by τ_{syn} and in amplitude by G_x. Equations (2), (3) and (4) together make our neuron model.

Note that it differs from that in [25], where instantaneous (conductance-based) were chosen instead

$$I^x_{syn}(t) = C[V_x - V(t)] \sum_{i,j} g_x \delta(t - t_{i,j}), \tag{5}$$

where g_x is a normalised amplitude of the synaptic conductance response and $\delta(t)$ is the Dirac delta function. Non-instantaneous synapses act as a low pass filter, smoothing out the discontinuous jumps in voltage.

The [25] model included variability in the pre-synaptic transmission delays of connections, *i.e.* distinct synapses had distinct transmission delays. This variability was introduced for two reasons. First, completely identical delays over all synapses is not a biologically realistic situation. Second, intra-link delay variability – *i.e.* variability in the delays on the connections that link two consecutive pools – has an effect on pulse packet propagation similar to that of non-instantaneous synapses. Indeed, the integration of inputs from an incoming volley of simultaneous spikes becomes non-instantaneous, which opens up a short time window during which background input can interfere with pulse packet propagation. This is important because regulation of the number of co-active waves was found in [25] to depend on this effect. Note however that such intra-link delay variability must be small in order to have propagation of waves; it is in fact a defining property of a synfire chain network. In contrast, differences between transmission delays on different pool-to-pool links can be large, without affecting pulse packet propagation.

Hence the model features synapses transmission delays made of two components. First, a large component, the so-called inter-link delay, that is the same for every synaptic connection within a given pool-to-pool link, but varies across links. Second, the intra-link transmission delay that varies across the synapses within each link. This component is kept small as explained above. Hence, one can write the synaptic transmission delay

between the ith neuron in the μth E-pool to the jth neuron in the next I/E-pool as

$$\tau(\mu, i, j) = \tau_A(\mu) + \tau_B(\mu, i, j), \tag{6}$$

where $\tau_A(\mu)$ is the inter-link, and $\tau_B(\mu, i, j)$ the intra-link component. For biological realism, the total transmission delay must follow a wide distribution; as a consequence, the inter-link delay variability is chosen large with respect to the intra-link delay variability. Numerically, $\tau_A(\mu)$ is uniformly distributed over $[0.5, 4.5[$, and $\tau_B(\mu, i, j)$ over $[0, 0.5[$.

Importantly, the second reason for intra-link delay variability – to act as a substitute for non-instantaneous synapses – does not apply to the current model since it uses non-instantaneous synapses. Nevertheless, our base protocols kept the intra-link transmission delay variability, but we also investigated what happens without it. On the other-hand, since inter-link delay variability plays no role in the propagation of waves, we kept it in all our simulations for biological realism purposes – and it is the main component of delay variability.

In order to choose parameters, for the current model, that will give behaviour comparable to that of the previous model [25], we need to relate their respective synaptic conductance amplitudes, namely g_E and G_E. One can do so by equalising the expected change in the membrane potential caused by one excitatory synaptic event in both models. We begin by integrating in the non-instantaneous case

$$\frac{\mathrm{d}V}{\mathrm{d}t} = \frac{1}{C}[V_E - V(t)]G_E \exp[-t/\tau^E_{syn}]. \tag{7}$$

Assuming $V(t)$ is constant over that time scale – which is a good approximation if we make the most unbiased assumption that all the other inputs we do not consider will leave $V(t)$ unchanged – it yields

$$\begin{aligned} \Delta V &= \frac{1}{C}[V_E - V] \int_0^\infty \mathrm{d}t G_E \exp[-t/\tau^E_{syn}], \\ &= \frac{1}{C}[V_E - V]G_E\tau^E_{syn}, \end{aligned} \tag{8}$$

while integrating the delta function in the instantaneous case yields

$$\Delta V = [V_E - V]g_E. \tag{9}$$

Hence the two amplitudes are related by

$$G_E = \frac{g_E C}{\tau^E_{syn}}, \tag{10}$$

allowing us to set the value of G_E in our model to be equivalent to the value of g_E used in [25].

2.1.3 Numerical simulations protocols and parameters

Our base protocol for simulating the network is somehow different than most similar network studies: as in [25], there is no ongoing external background excitatory input of the form of a continuous current or a Poisson external source at constant rate. This shows that synfire waves alone can sustain the ongoing activity present in the network.

External input arrives in the form of pulse packets of excitatory spikes, fed to a given E-pool and its I counterpart, in order to initiate a new wave. Such a stimulus occurs every 40 ms, starting at $t = 200$ ms. It consists of n_E spikes normally distributed in time, with mean t and standard deviation 0.1 ms, that are fed to each neuron of the two pools. Synaptic transmission delay for those connections are taken from the same distribution as the intra-link delay τ_B. These specifications ensure the external pulse packets impinge on their pools very similarly to what happens during internal wave propagation. Note that, for visualisation purposes, we always delivered those stimuli to the same pool (the zeroth pool). This does not, however, influence the behaviour our system.

In order to make sure that neurons in the system have a membrane potential close to the equilibrium potential rather than the resting potential when the first quasi-synchronous stimulus arrives, we deliver balanced I/E external Poisson background input – but only at the beginning of the simulation. The simulation begins with excitatory and inhibitory Poisson sources firing at a rate approximately equal to that produced by the propagation of 4 synfire waves. This is reduced in four steps to zero: the first step occurs at the same time as the first external pulse packet stimulus ; the 3 others, at each next one. Hence just after $t = 320$ ms, 4 pulse packets have been fed to the system, and the Poisson sources are turned off for the rest of the simulation. That way, firing rate fed to the system is approximately constant (if the stimuli initiate non-dying waves).

Values of the parameters are given in Tables 1-3. Most are the same as in [25], for the sake of continuity and comparison purposes. Their choice is based on physiological data. The simulation time was chosen to exceed any transient time sufficiently so as to allow the system to be at equilibrium long enough to characterise its properties.

Two other experimental protocols were used to study the effect of background input on the spontaneous emergence of waves. In both protocols, no wave were injected into the system. In the first protocol, we start the simulation with zero external Poisson input. Then, we feed the neurons with C_E Poisson sources, firing at rate increasing by 1 Hz every 50 ms. By the end of the simulation the external rate of the source is 100 Hz. We refer to this protocol as the ramping up. The ramping down, however, starts at 100 Hz and goes down to 0 Hz at the end of the simulation. The two protocols are designed to see the effect of background input on the spontaneous emergence of waves.

In order to detect pulse packets in all the experiments, we created a so-called "pulse

packet detector" neuron for each excitatory pool. Each neuron in any given pool is then linked to the associated detector neuron, which receives thus as many inputs as there are neurons in a pool. Hence, when a pulse packet arrives at a pool, most of its neurons will fire, yielding a sudden rise in the membrane potential of the detector neuron. With suitable parameter settings, the detector neuron will also fire, and thus we can record its spikes and interpret them as pulse packets. Each pulse packet detector is a leaky IAF neuron with instantaneous current-based synapses. The synaptic amplitudes are set to 1 mV and the distance from resting to threshold potentials to $n_E/2$ mV. Thus $n_E/2$ synchronous inputs will cause it to spike. Furthermore, its membrane time constant is set to a small value – $\tau_m = 2.5$ ms – so that approximately n_E inputs must arrive in near-synchrony in order to cause it to spike. With these settings, the pulse packet detector reliably responds to genuine pulse packets, and rarely responds to background asynchronous spiking in the pool (except in cases where the rate of such spiking becomes particularly high).

To compute the number of co-active ways in the system over time, we use the detected pulse packets in the following way. We link all pulse packets belonging to a given wave together, so as to end up with a list of waves ; one wave consisting of a start and an end pulse packets. In order to do so, we use an estimate of the propagation time T of pulse packets between two pools. For each pulse packet, we only search for the other pulse packets that belong to the next pool and that occur T ms (plus or minus a tolerance of 0.5 ms) after the packet considered. If no packet fulfils the condition, it means our packet is either at the end of wave, or it is a spurious one. If more than one packet satisfy the condition, that which is closest to the propagation time T is picked, and the temporary end of the wave it belongs to is updated. When we have a list with all starts and ends of waves, the number of waves at time t is obtained by counting the waves that start before t and end after it.

Computing the total firing rate from the data is trivial with the spike file we get from the simulations: one only needs to count the number of spikes. The firing rate due to pulse packets propagating, however, requires a more thoughtful method to be extracted. Indeed, we need to count the number of spikes belonging to pulse packets. In order to know if a spike belongs to a specific pulse packet (determined by a time and pool), we need to have the information about the pool the neuron belongs to. Hence, one need to have the *virtual* spikes instead of the real ones. We call real spike a pair composed of a spiking time and the neuron (one among the N_E) that produced it. For each real spike, there are as many virtual spikes as pools the *real* neuron belongs to. A virtual spike is a pair of a spiking time and a virtual neuron index that indicate to which (single) pool it belongs. Note that since a neuron belongs on average to pn_E/N_E, there will be that many more virtual spikes than real ones. Hence, counting the virtual spikes in pulse packets will give an overestimate of the actual number. One must subtract the contribution of the virtual spikes that belong to more than one pulse packet. We did so for a random sample of the pulse packets in the system at equilibrium, and deduced an average number

Parameter	Value	Units
C_m	250	pF
V_{rest}	-70	mV
V_E	0	mV
V_I	-80	mV
V_R	-70	mV
V_θ	-55	mV
t_{ref}	2	ms
τ^E_{syn}	0.5	ms
τ^I_{syn}	0.5	ms
τ_m	20	ms
g_E	0.005	–
G_E	2.5	nS

Table 1: Neuron model parameters

Parameter	Value	Units
C_E	8000	–
ϵ	0.1	–
γ	4	–

Table 2: Network structure parameters

Parameter	Value	Units
simtime	5000	ms
time step	0.1	ms

Table 3: Simulation parameters

of wave spikes per packet, allowing the computation of the associated rate. Note that the correction to the overestimate only becomes non-negligible at sufficiently high pool size. This explains why the overestimation was not detected in [25].

2.2 Mean field approach

In this section, we present the mean-field approach to explaining the behaviour of our SFCSN network. The mean field approach involves analysing the system in terms of a mean firing rate. Such an approach has been successfully used to describe balanced random networks (e.g. [7, 19]). As in [25], we use this mean-field approach as a means of predicting behaviours and instabilities in our SFCSN model.

We assume that our network can be globally characterised by its average firing rate ν. In our case of embedded SFCs, that firing rate has two components use; one due to what we call *stochastic spiking* of neurons, another due to their *wave spiking*

$$\nu = \nu_W + \nu_S. \tag{11}$$

Wave spiking is the firing of a neuron due to the arrival of a pulse packet from one of its predecessor pool or from an external source. Stochastic spiking is the firing due to *background input*, *i.e.* to all other sources of inputs; those not due to the arrival of a pulse packet. There exists excitatory and inhibitory background input at respective rates λ_E and λ_I. As per [25], the excitatory part is the total input coming to the neuron, minus the fraction of wave spiking that comes from pulse packets in all the neuron's preceding pools. Indeed, a neuron i belongs on average to C_E/n_E pools, and hence has as many preceding pools, each containing n_E neurons (see figure 1(b)). As expected, we fall back on our feet with a number of connections of C_E by multiplying the last two quantities. Each of the neurons in those preceding pools fire at a rate $\nu = \nu_W + \nu_S$. This adds up to a total firing rate of $(C_E/n_E)n_E(\nu_W + \nu_S)$. Now take a neuron j in one of those pools preceding that of neuron i. The component of its firing ν_W is due to pulse packets in all C_E/n_E pools it belongs to. Hence, the fraction of its ν_W it brings to neuron i is only that due that one pool – among the C_E/n_E – neuron j belongs to that precedes one pool neuron i belongs to, and hence reads $(C_E/n_E)^{-1}\nu_W$ times the number C_E of such neurons j. This can be summarised as

$$\begin{aligned}\lambda_E &= C_E(\nu_W + \nu_S) - n_E\nu_W, \\ &= C_E(\nu_W(1 - n_E/C_E) + \nu_S), \\ &\simeq C_E\nu,\end{aligned} \tag{12}$$

where the approximation stands valid when $n_E \ll C_E$. Since inhibitory pools do not take part in propagation of pulse packets, the inhibitory part of background input simply reads $\lambda_I = C_I\nu$. This is convenient because it ensures that the ratio $\lambda_I/\lambda_E = \gamma$ is kept constant in the analysis, and hence we need only one of the two parameters to describe the system.

Since by definition stochastic firing is a function of only background input, one can write

$$\nu_S = f_S(\lambda_E, \lambda_I), \tag{13}$$

and as a consequence of the constant excitatory:inhibitory ratio, as a function of the sole variable λ_E

$$\nu_S = \hat{f}_S(\lambda_E), \tag{14}$$

which is equivalently written

$$\nu_S = \hat{f}_S(C_E(\nu_W + \nu_S)), \tag{15}$$

based on equations (11) and (12), or in the form of a new function of the rates only

$$\nu_S = \tilde{f}_S(\nu_W + \nu_S). \tag{16}$$

This can be moreover understood as a self-consistency equation for our mean-field analysis: the stochastic spiking coming in is the same as that going out. Additionally, equation (16) can be viewed as an iterative map for ν_S, where at each new step, the output ν_S

is fed back into the function, with a fixed ν_W. Hence, it is possible to determine the equilibrium value for ν_S – for given values of the other parameters – as a the fixed point of the map. No analytical form for $\tilde{f}_S$ exists for our model, and we will discuss its numerical determination further in the text.

Other than causing stochastic firing, background input modulates pulse packets propagation. As mentioned in relation to transmission delay variability, background input interferes with wave propagation. As a result, there is an upper limit $\lambda_{E,max}$ on the rate of background input which will permit wave propagation along a chain of a given pool size. $\lambda_{E,max}$ increases with pool size, as calculated numerically in [25] – but not calculated here.

Similarly to stochastic spiking, wave spiking is a function of other system variables, given in [25] by

$$\nu_W = f_W(\lambda_E, \lambda_I, h, n_E) = \frac{h n_E p_f(\lambda_E, \lambda_I)}{N_E T(\lambda_E, \lambda_I)}, \tag{17}$$

where the influence of background input is explicit, and h is a fixed number of waves in the network. T denotes the mean pool-to-pool propagation time and p_f is essentially the probability that any given neuron in the pool contributes a spike to the packet.

Together, equations (11), (12), its I counterpart, and equations (13) and (17) constitute a complete system of equations for the three rates, given h. Moreover, since λ_I can be written in terms of λ_E, those can be combined to obtain an equation for λ_E as

$$\lambda_E = C_E \left(\frac{h}{N_E} \frac{n_E p_f(\lambda_E, \gamma\lambda_E)}{T(\lambda_E, \gamma\lambda_E)} + f_S(\lambda_E, \gamma\lambda_E) \right), \tag{18}$$

We evaluated the transfer function $\tilde{f}_S(\nu)$ by simulating a single neuron receiving input from C_I inhibitory and C_E excitatory Poisson sources at rate ν, and recording the output firing of that neuron.

The neuron we used was the same as those of the SFCSN. We also kept the same time resolution, but simulated for 5 times longer than the SFCSN, to improve the estimate of the firing rate. We simulated the SN for the same values of g_I as we did for the SFCSN. Determining the transfer function implies simulating the SN for various input rates. Hence, for a given g_I value, we simulated the SN for logarithmically-spaced values of the input rate ν, ranging from 0 to 400 Hz. Figure 2 illustrates the obtained output firing rates (blue dots) as a function of the input rate, which determines the transfer function.

Given the data, we interpolate it in order to have a continuous form for $\tilde{f}_S(\nu = \nu_W + \nu_S)$. To solve the fixed point equation (16), it is helpful to define the new function $f(\nu_S) =$

$\tilde{f}_S(\nu = \nu_W + \nu_S)$; then one can simply rewrite the equation as

$$\nu_S = f(\nu_S), \tag{19}$$

whose solution is the value of ν_S at the intersection between $f(\nu_S)$ and the identity function, as graphically depicted in figure 2. Note that, by definition, this new function f (red continuous line) is just the function $\tilde{f}_S$ whose x-axis was shifted by ν_W.

We used those simulations in two ways. First, we simulated the SN to help us find suitable g_I values for the SFCSN. Indeed, we wanted our network to be able to exhibit a low cortex-like stochastic firing rate, described as the AI regime by [7]. In order to do so, we simulated the SN for several g_I values, and used in the SFCSN those which would give a low equilibrium firing rate.

Second, we used it the other way around (from the SFSCN to the SN) to compare the mean field predictions with the SFSCN results. In order to do so, we started with the simulation of the SFCSN for a given pair of values (g_I, n_E). From the data produced, we determined the three rates ν, ν_W, and ν_S. Next, we simulated the SN for the same value of g_I, and determined the fixed point, using the value ν_W from the SFSCN. The fixed point would then give us a ν_S that we compared with that of the SFSCN.

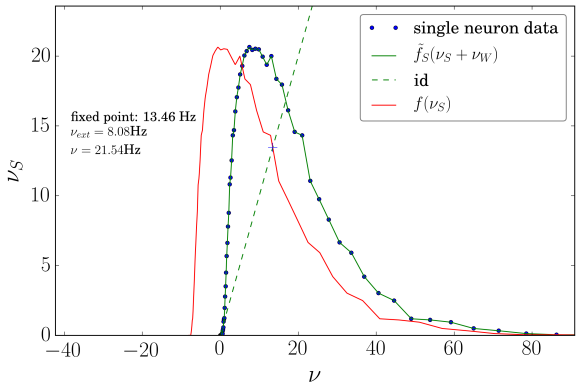

Figure 2: Illustration of the fixed point analysis procedure, based on data from simulating a single neuron for a given set of parameters.

3 Results

Results in this section were obtained by simulating our SFCSN model with the base protocol described in section 2.1.3. Exploration of the parameter space was conducted in the n_E-g_I plane, with values for n_E ranging from 60 to 800 – by steps of 20 – and between 0.077 and 0.053, by steps of 0.002.

First, we give, in figure 3, typical examples of behaviours that simulations of our SFSCN exhibit. Pulse packets, mean firing rate, and number of co-existing number of waves over time are shown. Every simulation tends to an equilibrium after some transient time, and we show the quantitative analysis of that equilibrium in the next paragraphs.

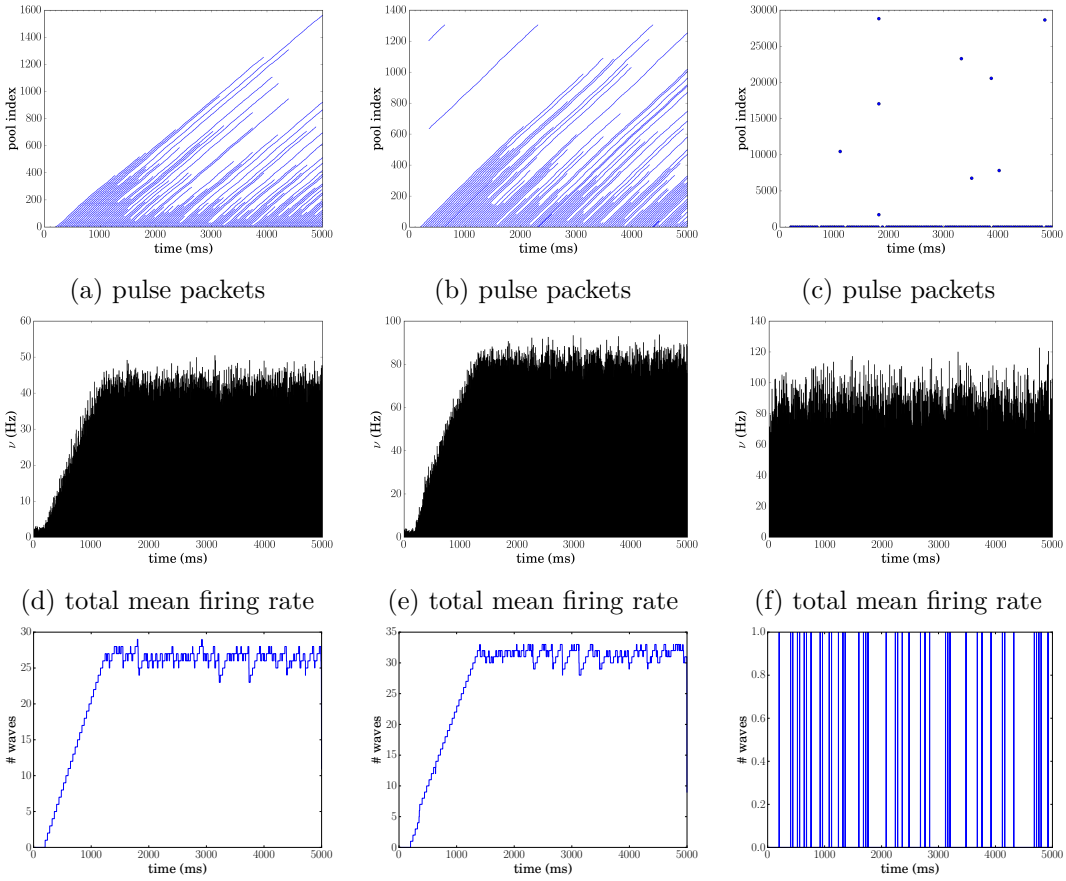

(a) pulse packets (b) pulse packets (c) pulse packets

(d) total mean firing rate (e) total mean firing rate (f) total mean firing rate

(g) waves number (h) waves number (i) waves number

Figure 3: Typical network simulation behaviours. Mean firing rate, number of co-active waves, and spikes raster of neurons for three parameters settings. (a,d,g): $n_E = 400$, $g_I = 0.077$; (b,e,h): $n_E = 700$, $g_I = 0.072$; (c,f,i): $n_E = 140$, $g_I = 0.053$.

3.1 Equilibrium state characteristics

The equilibrium state of our SFCSN can be described in terms of its mean total, stochastic, and wave spiking rates as explained in section 2.2. The evolution of those rates across the parameter space is shown as a function of pool size, for all values of g_I simulated, in

figure 4. From those figures, a clear distinction between two main regimes can be made. First, a regime where wave spiking is largely stronger than stochastic spiking, that we will thus call the synfire wave dominated regime (SFWD). SFWD occurs for example at $g_I = 0.073$ for all n_E larger than about 150 (see figure 4(c)). Second, a regime where, on the contrary, stochastic spiking dominates and the number of co-active wave in the system is approximately zero, which we refer to as the stochastic spiking dominated regime (SSD). SDD can be seen for example at $g_I = 0.073$ for all n_E less than about 150 (see figure 4(c)). Those two examples and figure 4 already show the importance of pool size and inhibition strength on the transition between the two regimes: the upper n_E bound for SSD increases as g_I decreases.

A more compact view of the regions where the two regimes occur is given in figure 5(a), where wave spiking is shown as a function of pool size, for an array of inhibition strength values. It is there visible where the transition occurs: at low g_I and n_E values. Indeed, ν_W is seen to drop to around zero in curves representing n_E values lower than 420. Just below that value, the transition is very steep: at $n_E = 360$, ν_W drops from about 75 Hz to just about 4 for g_I values of 0.055 and 0.053 respectively. Furthermore, the value of the inhibition strength at which the transition occurs depends on that of n_E. In fact, in that low n_E and g_I region, the lower the pool size, the smoother the decrease of waves spiking, and the larger the g_I value at which it occurs. As a comparison with the last example, at $n_E = 140$, ν_W decreases from just under 10 Hz to 0 and does so between respective g_I values of 0.069 and 0.061.

A more qualitative picture is given in figure 6, which gives an overview of the three rates across parameter space. The region for SSD is clearly distinguishable from the rest of the picture.

Several facets of the behaviour of the SSD regime are shown in figure 3(c,f,i): the total firing rate, the number of waves, as well as pulse packets over time. As shown in previous graphs, this regime is exhibited at low g_I and n_E, and the upper bound on pool size of the region where it appears decreases as g_I increases. The SSD regime is characterised by a domination of stochastic spiking over wave spiking, as the name tells. The mean number of co-active waves at equilibrium is approximately zero – e.g. 0.02 for $g_I = 0.053$ and $n_E = 140$, with only small fluctuations around zero. Neurons start to fire near their equilibrium total rate immediately at the start of the simulation – at 85 Hz for the same parameters as above – unlike in the SFWD regime. The approximately null number of co-active waves in the SSD regime is a consequence of the non-robust propagation of those waves, as shown in figure 3(c).

As g_I is decreased, two opposing effects come into play. First, it shifts the I/E balance of background input, which makes background input less destabilising to wave propagation. As a result, waves can tolerate more background input and hence the total firing rate rises. Second, however, weaker inhibitory strength yields more stochastic spiking. The

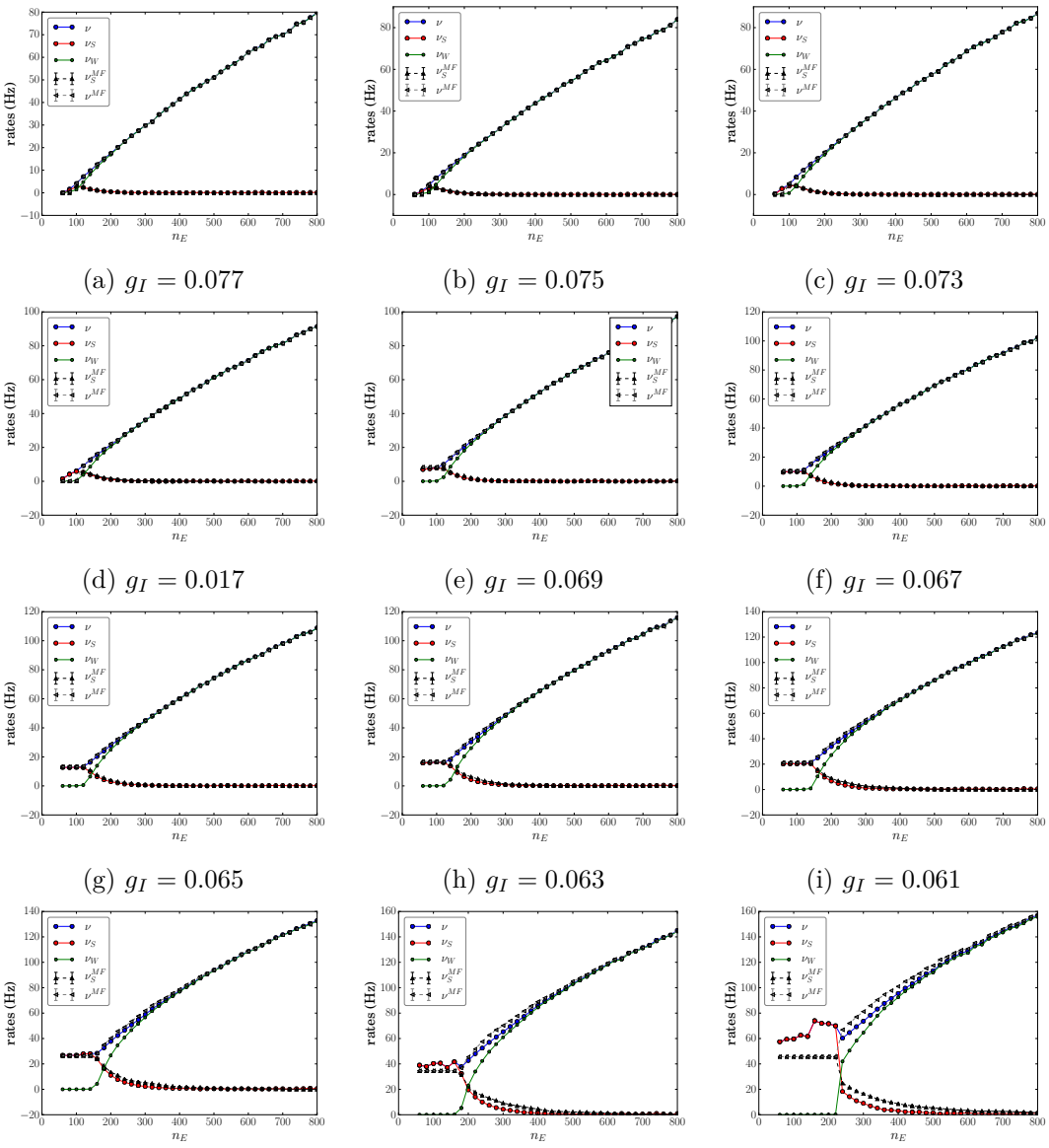

(a) $g_I = 0.077$ (b) $g_I = 0.075$ (c) $g_I = 0.073$

(d) $g_I = 0.017$ (e) $g_I = 0.069$ (f) $g_I = 0.067$

(g) $g_I = 0.065$ (h) $g_I = 0.063$ (i) $g_I = 0.061$

(j) $g_I = 0.059$ (k) $g_I = 0.057$ (l) $g_I = 0.055$

Figure 4: ν, ν_W, and ν_S as functions of pool size, each for a particular value of g_I, together with the mean field predictions for ν and ν_S. Error bars on those two quantities are very small and hence hardly distinguishable

relative strength of those two effects finally determine ν_W, which is equal to the total firing rate minus the stochastic firing rate. Our results show that in the SSD regime, the increase in ν_S strongly outweighs that in ν, yielding zero wave spiking.

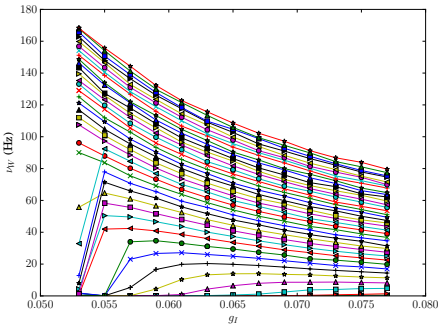

(a) Wave spiking as a function of inhibition strength, for all values of pool size ; the top curve is for $n_E = 800$ and that at the bottom for $n_E = 60$, with curves in between every step of 20. The breakdown of ν_W is clear for small-sized pools at lower g_I.

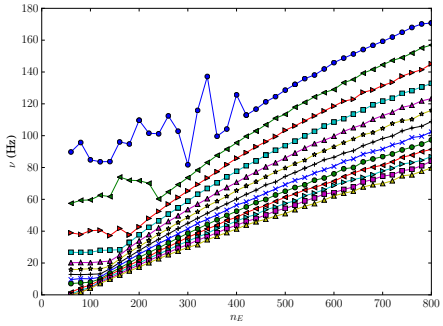

(b) Total mean firing rate as a function of pool size, for all values of g_I ; the top curve is for $g_I = 0.053$ and that at the bottom for $g_I = 0.077$, with curves in be tween every step of 0.002.

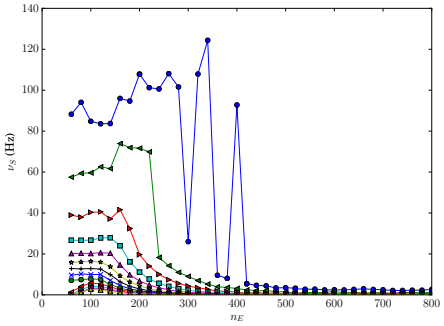

(c) Stochastic firing rate as a function of pool size, for all values of g_I ; the top curve is for $g_I = 0.053$ and that at the bottom for $g_I = 0.077$, with curves in between every step of 0.002.

Figure 5: Total firing rate and its components across parameter space.

As mentioned earlier, our initial choice of parameters – that led to SFWD behaviour – was suggested by the values used in the model in [25]. The SFWD regime exhibits different qualitative behaviour to that of the SSD regime. By our definition of it, all spiking is stochastic. Waves propagate through many pools, showing stable propagation, in contrast to SSD. There is a long transient to equilibrium as waves are fed into the system and the number of waves increases. After the transient, a trade-off for the two opposite effects of background input is found: its destabilising and promoting effects on wave propagation equilibrate, *i.e.* the number of waves dying counter-balance that of waves coming into the system. In other words, regulation of the number of waves happens, just as in [25].

SFWD is found for all of the explored region except at low n_E and g_I where SSD prevails, as discussed. Across the SFWD region, varying pool size or inhibition strength affects

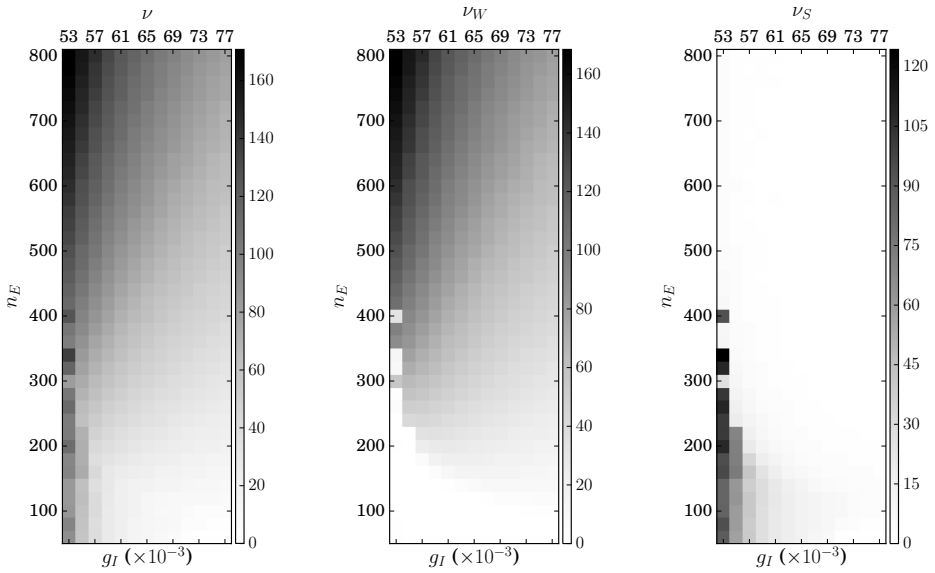

Figure 6: Grayscale plot of the three different rates across the plane simulated in the parameter space.

the values of the rates and wave propagation. Indeed, as n_E is varied to higher values across that region for a given value of g_I, waves propagate through more pools before extinguishing, indicating a higher survival probability, and hence more stable propagation. Additionally, the total mean firing rate goes up too, just as the number of co-active waves does. Note that as a result of a more stable propagation, the number of waves fluctuates with smaller amplitudes around its mean value. In fact, the more stable propagation is, the less often do several waves die at the same time.

Data shows that, in contrast to the SSD case, for sufficiently high values of n_E, the net result of a decrease of g_I is an increase of ν_W. An increase in pool size leads to an increase in both ν and ν_W, whereas ν_S is staying close to zero. Such an increase is expected to have two effects. First, higher pool size yields more robust wave propagation, and hence an increase of ν_W. In turn, this will increase background input which has a destabilising effect on wave propagation, as stated earlier. Results of our model show that, for sufficiently high values of n_E, the wave promoting effect outweighs the other, resulting in a net increase of wave spiking and total spiking rates.

Our mean field theory describes reasonably well the equilibrium rates of our system across parameter space, as shown in figure 4. They are obtained by the fixed-point analysis described in section 2.2, based on the transfer function of a single neuron shown in figure 7, which we will discuss later.

Error bars shown on the graphs are very close to zero and hence not easily seen. Despite the fact that the single neuron simulations gave rates that match those from the SFCSN simulations, some systematic deviation appears approximately between pool sizes of 200 and 400, where the mean field overestimates both ν and ν_S. These deviations increase as g_I decreases. This deviation may come from the fact that in simulations of the network, wave and stochastic spiking interfere. Also, the lower the inhibition, the more spikes, and hence the more interference. This is an effect that is not captured in the mean field approach.

It is important to note the significant difference of the transfer function of our neuron in comparison with that in [25]. In fact it is non-monotonic: it first rises as input rate does, but then reaches a maximum and decreases as the input rate still increases. This behaviour is characteristic of non-instantaneous conductance-based neurons [16], and has not been observed in any of the simpler synaptic models (instantaneous or current-based or both). This has a significant impact on the network dynamics; indeed, it means that for a given g_I value, there is a maximum stochastic firing rate. This is in marked contrast with neurons exhibiting monotonic functions, as there is no upper limit on the stochastic firing rate as background input increases, other than that imposed by the refractory period: 500 Hz. This ensures better stability of the low rate AI stochastic spiking as long as that maximum is sufficiently low.

Most importantly, it the non-monotonic nature of the transfer function that leads to the existence of the SSD regime. Indeed, the SSD regime corresponds to a non-zero fixed point even for zero synfire waves or external input, meaning it is a self-sustained state (as was also found in a BRN with non-instantaneous conductance-based synapses in [17]). Such a fixed point does not exist in models with a monotonic transfer function [25]. Transition from the SFWD regime to the SSD one can be understood as the switch from a regime in which synfire stability determines the equilibrium of the system, to one in which self-sustaining stochastic spiking alone exists.

The transition to the SSD as n_E decreases can be understood as the combination of the effect of the non-monotonic transfer function and the dependence of $\lambda_{E,max}$ on n_E. Indeed, as the pool size decreases, so does $\lambda_{E,max}$ which is related to the equilibrium firing rate [25] by $\nu = \lambda_{E,max}/C_E$. Hence, as n_E decreases, ν decreases too, but ν_S increases. At a critical pool size, ν and ν_S become equal and equivalently $\nu_W = 0$. This phenomenon can be seen in figure 4.

The single neuron transfer function is computationally easier to obtain at low g_I values than complete SFCSN simulations. Hence, they can be used to make predictions about the behaviour of our network at g_I values we did not simulate. The curves in figure 7 go down to values of 0.045, and suggest that there will be no sudden change to a high activity state as those witnessed in [25]. Indeed, the maximum of the functions appears to continually increase, indicating no possible important jump to a high activity state.

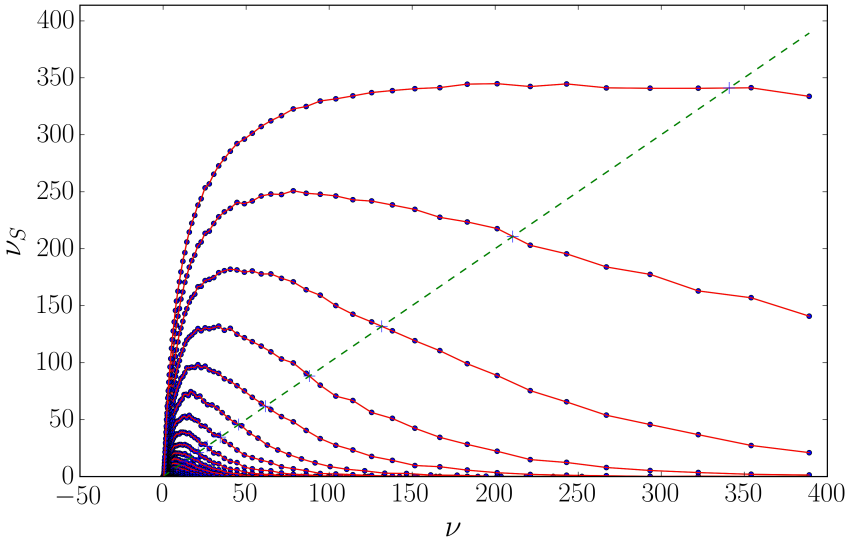

Figure 7: Transfer function of a single neuron: output firing rate as a function of the input rate. The green dashed line is the identity function. The highest curve is for $g_I = 0.045$, and the lowest for $g_I = 0.077$, with a curve for intermediate values every 0.002 units.

3.1.1 Embedding capacity

Embedding capacity of our model is very similar to that found in [25]. A trade-off exists between firing rate and embedding capacity. Results show an embedding capacity α_{max} between 0.8 and 1 for an equilibrium firing rate of 5 Hz , and of approximately 0.55 for an equilibrium firing rate of 10 Hz. This is in good agreement with what was found in the model in [25].

3.2 Spontaneous wave births

As n_E is increased, spontaneous wave births start to appear, as illustrated in figure 3(b). Hence losing the stability of the ground state. Note that in these experiments, spontaneous wave births only occurred early in the simulations: either at the very start, or closely after the first wave was injected (see figure 3(b)). The former only appears for lower values of inhibition strength whereas the latter appears for higher values of the same parameter. As a consequence of their appearance only early in the simulations, they did not seem to have any influence on the equilibrium rates that could not be captured by the mean field approach.

In order to try and better understand the conditions for spontaneous wave births, we conducted ramping up and ramping down experiments, as defined in section 2. As in [23], it appears that spontaneous wave births depends on background input and pool size. Given a value of background input, there is upper bound on n_E above which waves spontaneously emerge. This value decreases as λ_E increases. Our results for the ramping down experiments show the same characteristics. The lower the pool size, the more background input is needed to induce spontaneous births. Also, for a given n_E, the more background input, the more waves appear as long as the background input stays at that level. Hence, spontaneous waves only appear towards the end of the simulations, when the firing rate is high enough. This is in contrast with happens in the ramping down experiments, where spontaneous births occur at the beginning. However, the contrast is that no more waves appear after that, even if background input increases even more, or goes back to the value inducing the births. The difference between ramping up and down results is illustrated in figure 8.

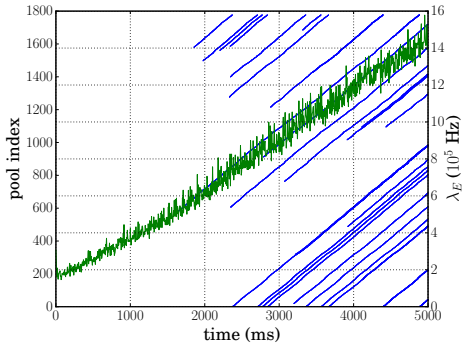

(a) Waves spontaneously appear over a range of values for background input.

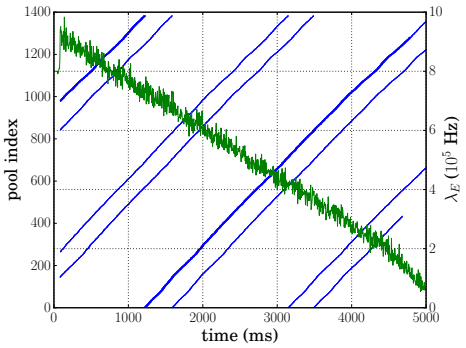

(b) Waves spontaneously appear once when a certain background input value is reached, but not after that.

Figure 8: Ramping up (a) and down (b) experiments.

The only conclusion drawn from those results is that spontaneous births of waves occur above a minimal pool size and background input. In order to better understand the mechanism, more focused experiments could be designed, as that in [25] studying the effect of background input on an isolated SFC. Another enhanced protocol would be to use many short chains, instead of the long cyclic one that was used. That way, if spontaneous births occur, the waves die very quickly and do not influence the spontaneous emergence of other waves through the increase in background input they cause.

3.3 Zero intra-link delay spread

Simulations of our SFCSN model with zero intra-link delay spread show two things. First, that non-instantaneous synapses are sufficient for the number of waves to be regulated, as was suggested in [25]. This is in contrast with the model in [25] and its instantaneous synapses, where the intra-link delay variability was found to be a necessary condition for the regulation of the number of waves. This was ensured by the destabilising effect of the intra-link delay spread on wave propagation, due the increased time spread of the propagating packets. Second, we see that the enhanced wave stability permitted by the zero intra-link delay spread in our model pushes the transition of the network to the SSD regime to lower values of g_I and n_E. This is illustrated in figure 9 where the propagation of pulse packets is compared, for the same parameters settings, between zero and non-zero intra-link delay variability. Finally, it appears this zero intra-link delay spread allows higher embedding capacity, as suggested in [25]. This, however, should be further investigated.

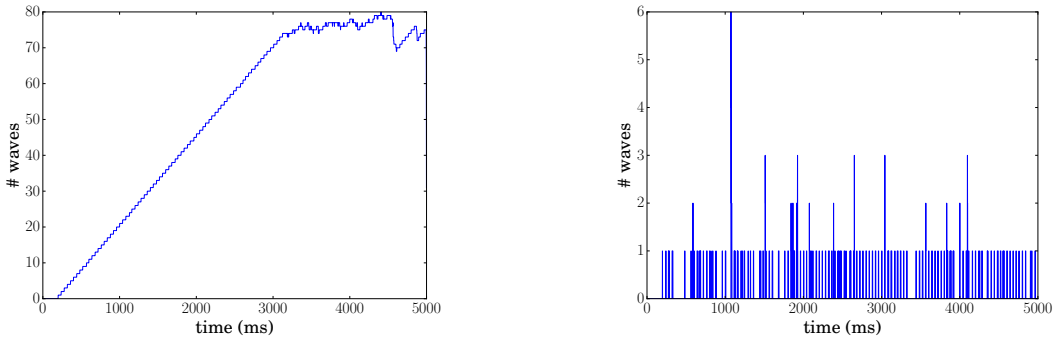

(a) Zero intra-link delay spread. The network is in the SFWD regime.

(b) Non-zero intra-link delay spread. The network is in the SSD regime.

Figure 9: Comparison of SFSCN behaviour between zero (a) and non-zero (b) intra-link delay spread, for $n_E = 220$ and $g_I = 0.053$.

4 Discussion

We presented a model of sequences of pools of neurons linked in a feed-forward fashion – synfire chains – embedded in a cortical network, on the basis of that presented in [25]. The difference of the current model with the previous one is the use of non-instantaneous conductance-based synapses rather than instantaneous conductance-based ones.

We studied the behaviour of the network across the g_I-n_E plane of the parameter space. High values for pool size were looked into: up to 800, as opposed to only 220 in [25].

We conducted numerical simulations of the network. We also gave a mean field analysis that describes the three firing rates at equilibrium: total, stochastic, and wave firing rates. Stochastic firing is due to quasi-random fluctuations of the membrane potential of the neurons, whereas wave spiking is due to pulse packets propagation along the synfire chain.

We looked for possible instabilities of the system's key properties that are necessary for it to be functionally relevant. Such key properties are the stability of synfire wave propagation along the synfire chain, and the stability of the low rate AI regime of all neurons in the network. Stability of the former is found to be lost below a lower bound on pool size and on inhibitory synaptic strength.

Beyond that limit, a first regime – stochastic spiking dominated (SSD) – was found, where wave propagation is not possible, and is dominated by quasi-random spikes. It is known that reduced inhibition can have two opposite effects on the network. As already explained, it increases stochastic spiking on the one hand, and increases the total firing rate on the other as a consequence of a less destabilising background input for wave propagation. It appears that in this model, below the limit on pool size and inhibitory synaptic strength, the former dominates the latter. This regime is new: it was not observed in [25]. Note that its existence is detrimental to the use of SFCs for composition, as composition is best with small pool-sized chains (large pools are inefficient).

A second regime was observed: the synfire wave dominated (SFWD) regime where wave propagation is robust, and largely dominates stochastic spiking that stays close to zero. This regime was also observed in [25] and is that which is functionally relevant. In this region of the parameter space, a trade-off is found for pool size and inhibitory synaptic strength that allows balance between the two aforementioned opposite effects. As explained in [25], the minimum pool size necessary for stable propagation of waves increases with background input. Self-regulation thus emerges as natural consequence. Self-regulation is a key property of both the model in [25] and this.

The mean field analysis described reasonably well the three equilibrium rates across state space. It accounted for the two aforementioned regimes, as well as the transition between them. This showed the suitability of such an analysis to our type of model, as in [25]. There is some systematic deviation between the mean field predictions and the network simulations, however. This happens mostly at pool sizes where the transition between the two regimes occur, and stochastic and wave spiking co-exist. Hence, it suggests the deviations are due to interference between those two rates, as was already suggested in [25]. Indeed, the mean field analysis does not account for such interferences.

Most importantly, it is the non-monotonic transfer function of our non-instantaneous conductance-based synapses that allows the existence of the SSD regime. Indeed, there exists a non-zero fixed point for zero synfire wave activity or zero external input. This

results in the possibility of a self-sustained regime where all spiking is stochastic. This non-monotonic shape also suggests there will be no sudden to a high activity state (similar to the exit of the inhibition dominated regime in [7]). This is in contrast to what was expected from the model in [25]. Additionally, the transition to the SSD regime as n_E is decreased can be understood as a combination of the aforementioned phenomenon combined with the effect of the dependence of $\lambda_{E,max}$ on n_E, and its direct relation with the total equilibrium firing rate. As n_E is decreased, $\lambda_{E,max}$ decreases too, yielding a decrease of the total firing rate while stochastic spiking rises. At some critical pool size, ν and ν_S become equal, meaning $\nu_W = 0$. We also verified that the embedding capacity of the model was similar to that in [25].

At very low g_I values, the curves obtained for the rates become very shaky. Indeed, as n_E increases, there is a region of parameter space where the system switches between the SSD and the SFWD regimes. This could hypothetically indicate the existence of bistability, where the system would reach one regime or the other if we were to repeat its simulation. This is, however, only a hypothesis, and the question of what happens at even lower g_I is left for future work.

Loss of the stability of the ground state of the SFC was seen above an upper bound on pool size: spontaneous wave births occur. This upper bound decreases with g_I. Ramping experiments confirmed spontaneous births depend on those parameters as in [23], but a more detailed understanding of the phenomenon could not be reached. Other experimental designs more targeted toward that question are required, such as the study an isolated SFC, or many short embedded ones, and this is left for future work.

The introduction of non-instantaneous synapses was motived by their suggested effect on the regulation of wave propagation, which is similar to that of intra-link delay variability. We simulated our SFCSN with zero intra-link delay spread, and saw regulation of the number of wave persist, as suggested in [25]. Moreover, the more robust propagation of waves pushed the border of the transition to the SSD regime. Further work is required to have a good quantitative description of the border, as well as an more precise idea about the allowed embedding capacity which seems to be higher than with intra-link delay variability, as suggested in [25] too.

It should be noted that, even though evidence for precise firing patterns exists, e.g. [4], the synfire chain hypothesis remains hard to test experimentally [13]. Indeed, this would require to be able to record from numerous neurons simultaneously, and that those neurons should belong to the same chain, or at least to mutually activating chains. Moreover, those chains should be under conditions for repeated activation. Given this, and that present recording techniques can record from no more than about 500 neurons simultaneously, failure of present techniques to detect SFC are inconclusive, and one must wait for better techniques or tools.

Additionally, the SFC hypothesis assumes that synfire chains can be formed through biological processes. Whether such mechanisms exist is still an open question, however. Approaches based on spike-timing dependent plasticity have been tried, but none of them are entirely successful. The model in [26] achieved formation of feed-forward structures but not for realistic cortical scales. Another recent work [18] – the only one of the kind at a cortically realistic scale to date – did not achieve formation of such structures, but this does not prove that it is not possible. Further studies are required to conclude on the matter.

In conclusion, we considered a model of synfire chain embedding at cortical scale, based [25], and looked for possible instabilities. In contrast the with previous study, we used non-instantaneous conductance-based synapses. Moreover, we went further in the exploration of the parameter space. We observed two distinct regimes dominated by either wave spiking (SSD) or stochastic spiking (SFWD). The latter is similar to what is seen in [25] and holds the same key features. The SSD regime, on the contrary, is new, and is due to the non-monotonic nature of the neuron transfer function, which allows the existence of a self-sustained non-saturated rate for stochastic spiking, even in the absence of waves or external input. Finally, we showed non-instantaneous conductance-based synapses are sufficient – and intra-link delay spread is not necessary – for wave regulation.

Acknowledgements The NEST simulation software was used for all our network simulations. The hardware used to run them was Juelich's Hambach computing cluster. We appreciated the opportunity to use it. Thanks to Cees van Leeuwen for having me in his group. Finally, many thanks to Chris Trengove for his guidance, patience, and time ; it was greatly appreciated.

References

[1] M Abeles, H Bergman, E Margalit, and E Vaadia. Spatiotemporal firing patterns in the frontal cortex of behaving monkeys. *Journal of neurophysiology*, 70(4):1629–1638, 1993.

[2] Moshe Abeles. Time is precious. *Science*, 304(5670):523–524, 2004.

[3] Moshe Abeles. Synfire chains. *Scholarpedia*, 4(7):1441, 2009.

[4] Moshe Abeles et al. *Local cortical circuits*. Springer, Berlin, 1982.

[5] Yuval Aviel, David Horn, and Moshe Abeles. Memory capacity of balanced networks. *Neural Computation*, 17(3):691–713, 2005.

[6] Yuval Aviel, Carsten Mehring, Moshe Abeles, and David Horn. On embedding synfire chains in a balanced network. *Neural computation*, 15(6):1321–1340, 2003.

[7] Nicolas Brunel. Dynamics of sparsely connected networks of excitatory and inhibitory spiking neurons. *Journal of computational neuroscience*, 8(3):183–208, 2000.

[8] Anthony N Burkitt. A review of the integrate-and-fire neuron model: I. homogeneous synaptic input. *Biological cybernetics*, 95(1):1–19, 2006.

[9] Anthony N Burkitt. A review of the integrate-and-fire neuron model: Ii. inhomogeneous synaptic input and network properties. *Biological cybernetics*, 95(2):97–112, 2006.

[10] Anthony N Burkitt, Hamish Meffin, and David B Grayden. Study of neuronal gain in a conductance-based leaky integrate-and-fire neuron model with balanced excitatory and inhibitory synaptic input. *Biological cybernetics*, 89(2):119–125, 2003.

[11] Markus Diesmann, Marc-Oliver Gewaltig, and Ad Aertsen. Stable propagation of synchronous spiking in cortical neural networks. *Nature*, 402(6761):529–533, 1999.

[12] Apostolos P Georgopoulos, Andrew B Schwartz, and Ronald E Kettner. Neuronal population coding of movement direction. *Science*, 233(4771):1416–1419, 1986.

[13] George Gerstein, Elizabeth Williams, Markus Diesmann, Sojna Grün, and Chris Trengove. Detecting synfire chains in parallel spike data. *Journal of Neuroscience Methods*, 206:54–64, 2010.

[14] Marc-Oliver Gewaltig and Markus Diesmann. Nest (neural simulation tool). *Scholarpedia*, 2(4):1430, 2007.

[15] Marc-Oliver Gewaltig, Markus Diesmann, and Ad Aertsen. Propagation of cortical synfire activity: survival probability in single trials and stability in the mean. *Neural networks*, 14(6):657–673, 2001.

[16] Alexandre Kuhn, Ad Aertsen, and Stefan Rotter. Neuronal integration of synaptic input in the fluctuation-driven regime. *The Journal of neuroscience*, 24(10):2345–2356, 2004.

[17] Arvind Kumar, Sven Schrader, Ad Aertsen, and Stefan Rotter. The high-conductance state of cortical networks. *Neural computation*, 20(1):1–43, 2008.

[18] Susanne Kunkel, Markus Diesmann, and Abigail Morrison. Limits to the development of feed-forward structures in large recurrent neuronal networks. *Frontiers in computational neuroscience*, 4, 2010.

[19] Hamish Meffin, Anthony N Burkitt, and David B Grayden. An analytical model for the 'large, fluctuating synaptic conductance state'typical of neocortical neurons in vivo. *Journal of computational neuroscience*, 16(2):159–175, 2004.

[20] Carsten Mehring, Ulrich Hehl, Masayoshi Kubo, Markus Diesmann, and Ad Aertsen. Activity dynamics and propagation of synchronous spiking in locally connected random networks. *Biological cybernetics*, 88(5):395–408, 2003.

[21] Luigi M Ricciardi. *Diffusion processes and related topics in biology*. Berlin: Springer-Verlag, 1977.

[22] Sven Schrader, Markus Diesmann, and Abigail Morrison. A compositionality machine realized by a hierarchic architecture of synfire chains. *Frontiers in computational neuroscience*, 4, 2010.

[23] Tom Tetzlaff, Theo Geisel, and Markus Diesmann. The ground state of cortical feed-forward networks. *Neurocomputing*, 44:673–678, 2002.

[24] Tom Tetzlaff, Abigail Morrison, Theo Geisel, and Markus Diesmann. Consequences of realistic network size on the stability of embedded synfire chains. *Neurocomputing*, 58:117–121, 2004.

[25] Chris Trengove, Cees van Leeuwen, and Markus Diesmann. High-capacity embedding of synfire chains in a cortical network model. *Journal of computational neuroscience*, 34(2):185–209, 2013.

[26] Amelia Waddington, Peter A Appleby, Netta Cohen, et al. Emergence of synfire chains with triphasic spike-time-dependent plasticity. *BMC Neuroscience*, 12(Suppl 1):P41, 2011.